Modelling of Scintillation at Radio and Optical Frequencies from Radiosonde Observations

Florian Quatresooz*, Danielle Vanhoenacker-Janvier‡, Claude Oestges§
ICTEAM - Université catholique de Louvain - Louvain-la-Neuve, Belgium
*florian.quatresooz@uclouvain.be, ‡danielle.vanhoenacker@uclouvain.be, §claude.oestges@uclouvain.be

***Abstract*—The future of Earth-to-space communications relies on the use of higher radio-frequencies and optical frequencies. For such frequencies, tropospheric turbulence starts to have deleterious effects, leading to important phase variations and amplitude scintillation. Those effects can be described thanks to the knowledge of vertical profiles of the refractive index structure parameter C_n^2. In this work, two approaches relying on radiosonde measurements are presented to obtain radio-frequency and optical C_n^2. Theoretical developments highlighting the contribution of humidity to radio-frequency scintillation are presented. This contribution is also illustrated with high resolution radiosonde data at Trappes (France) and Hilo (HI, USA). Obtained C_n^2 profiles are in agreement with the literature and will be validated with measurements at millimeter waves in the future.**

***Index Terms*—Tropospheric scintillation, optical turbulence, millimeter waves, Free Space Optics, radiosonde.**

I. Introduction

Propagation of electromagnetic waves for ground-to-satellite communications is impacted by Earth's atmosphere, leading to several well-known effects: attenuation of the signals due to gases and hydrometeors, depolarization of the waves, or scintillation. Scintillation arises from variations of the atmospheric refractive index along the propagation path due to atmospheric turbulence. It leads to fluctuations of the received amplitude and phase of the electromagnetic waves. At radio-frequencies above a few GHz (e.g. including millimeter waves and microwaves), tropospheric scintillation starts to have important effects, especially for low-elevation angles [1], [2].

In order to characterize and predict scintillation effects, several models describing the scintillation variance σ_χ^2 have been developed. Statistical models of σ_χ^2 and its distribution have been presented [3], [4]. Other models rely on the refractive index structure parameter C_n^2, linking the scintillation variance to a C_n^2 profile of the altitude with [5]

$$\sigma_\chi^2 \;=\; 42.48 \frac{k^{7/6}}{(\sin(\theta))^{11/6}} \int_{\text{height}} C_n^2(z) z^{5/6} \mathrm{d}z, \qquad (1)$$

where σ_χ^2 is expressed in dB^2, $k = \frac{2\pi}{\lambda}$ with λ the wavelength, z is the altitude above ground and θ is the elevation angle.

Hence, description of tropospheric scintillation is achieved thanks to the knowledge of C_n^2 profiles. Following the work of Tatarskii, C_n^2 models involving meteorological quantities such as pressure, temperature and humidity have been presented [6], [7]. In order to obtain those meteorological data, radiosondes are often used [8]. Alternatively, due to the low resolution of radiosonde data, probabilistic approaches were developed [9], [10]. However, in recent years, high resolution radiosonde measurements are becoming available worldwide, sometimes offering a vertical sampling distance smaller than 10 meters in the troposphere. They are thus of particular interest to revisit C_n^2 models based on radiosonde data [1].

Furthermore, major progress has also been made recently for characterizing optical turbulence and scintillation, especially for ground-based astronomy [11] and for free space optical (FSO) communications [12]. Since optical scintillation has the same origin as radio-frequency (RF) scintillation, both fields can benefit from each other. Comparison between RF and optical C_n^2 has been conducted in [13] and [14], showing that most differences are related to humidity fluctuations. In this paper, a further attempt to merge those two domains is presented, providing a simple C_n^2 model that can be applied to both fields.

Section II provides the mathematical developments leading to the definition of the refractive index structure parameter C_n^2. It also presents the main differences between radio-frequencies and optical frequencies. Then, Section III details two different models to extract C_n^2 based on its statistical definition. Finally, those models are applied to radiosonde measurements at Trappes (France) and Hilo (HI, USA) in Section IV.

II. Theoretical developments

The atmospheric refractive index n can be expressed as a function of macroscale atmospheric quantities [15]

$$n \;=\; 1 + 10^{-6}\, \frac{77.6}{T} \left(p + \frac{4810e}{T} \right), \qquad (2)$$

where T is the temperature in kelvin, p is the atmospheric pressure in hectopascal and e is the partial pressure of water vapor in hectopascal. Equation (2) is an approximation of a more general expression presented in [15], valid only in the temperature range from -50 to 40°C. This range approximately corresponds to temperatures observed in Earth's troposphere and stratosphere. Furthermore, in the following, (2) will be referred to as the refractive index definition for

radio-frequencies, valid for frequencies ranging from 1 MHz to 30 GHz [16]. It is also often adapted to express the refractivity N, defined by $N = (n-1) \times 10^6$.

Fluctuations of the refractive index are related to fluctuations of temperature, water vapor and pressure thanks to [17]

$$\mathrm{d}n \;=\; \frac{\mathrm{d}n}{\mathrm{d}T}\mathrm{d}T + \frac{\mathrm{d}n}{\mathrm{d}e}\mathrm{d}e + \frac{\mathrm{d}n}{\mathrm{d}p}\mathrm{d}p. \tag{3}$$

Defining the following quantities

$$a \;=\; \frac{\mathrm{d}n}{\mathrm{d}T} \;=\; -10^{-6}\frac{77.6}{T^2}\left(p + \frac{9620e}{T}\right), \tag{4}$$

$$b \;=\; \frac{\mathrm{d}n}{\mathrm{d}e} \;=\; 10^{-6}\frac{3.73\times 10^5}{T^2}, \tag{5}$$

$$c \;=\; \frac{\mathrm{d}n}{\mathrm{d}p} \;=\; 10^{-6}\frac{77.6}{T}, \tag{6}$$

and denoting deviations from the mean by n', T', e' and p', the fluctuations of n are given by [17]

$$n' = aT' + be' + cp'. \tag{7}$$

The definition of the refractive index structure function $D_n(\rho)$ is

$$D_n(\rho) \;=\; \left\langle \left(n'(\boldsymbol{r}+\boldsymbol{\rho}) - n'(\boldsymbol{r})\right)^2 \right\rangle, \tag{8}$$

with $\boldsymbol{r}$ the position in space and $\rho = |\boldsymbol{\rho}|$ the distance separating the two points where the structure function is evaluated. The notation $\langle\cdot\rangle$ depicts the mean, expressed as an ensemble average. Equation (8) relies on the local homogeneity and isotropy hypotheses of the refractive index field [5]. Equivalently, expressions for the temperature structure function $D_T(\rho)$, the partial pressure of water vapor structure function $D_e(\rho)$, and the pressure structure function $D_p(\rho)$ are obtained, as well as expressions of the cross-structure functions (e.g. $D_{Te}(\rho)$, $D_{Tp}(\rho)$, etc.).

Using (7), the refractive index structure function can be related to other structure functions, as detailed in [17],

$$\begin{aligned} D_n(\rho) = {} & a^2\; D_T(\rho) + b^2\; D_e(\rho) + c^2\; D_p(\rho) \\ & + 2ab\; D_{Te}(\rho) + 2ac\; D_{Tp}(\rho) + 2bc\; D_{ep}(\rho). \end{aligned} \tag{9}$$

This result is of particular interest to determine the link between the structure parameters of the different quantities. Indeed, according to the Kolmogorov theory of turbulence [5], [6], the refractive index structure function is equal to

$$D_n(\rho) = C_n^2\; \rho^{2/3}, \tag{10}$$

in the inertial range, with C_n^2 being the refractive index structure parameter at radio-frequencies. Assuming a similar form for the other structure functions and using (9), C_n^2 can be expressed as

$$\begin{aligned} C_n^2 = {} & a^2\; C_T^2 + b^2\; C_e^2 + c^2\; Cp^2 + \\ & + 2ab\; C_{Te} + 2ac\; C_{Tp} + 2bc\; C_{ep}. \end{aligned} \tag{11}$$

Equation (11) is presented in [17], and, as already pointed out by [18], is valid as long as the dependency in ρ is the same for all structure functions (hence, not necessarily $\rho^{2/3}$).

Pressure fluctuations are found to be one order of magnitude smaller than temperature or humidity fluctuations [16], [17]. Therefore, they are usually neglected in (11), leading to

$$C_n^2 = a^2\; C_T^2 + b^2\; C_e^2 + 2ab\; C_{Te}. \tag{12}$$

This last results is often found in the literature, sometimes expressed with the specific humidity q [kg/kg] instead of the partial pressure of water vapor e [13]. These two quantities are linked by $e = 1.62\; pq$.

Nevertheless, in a recent paper, Cherubini recommends the use of conservative additives when expressing the refractive index structure parameter [7]. In this case, the temperature T must be substituted by the potential temperature θ, using the following relation

$$\theta = T\left(\frac{p_0}{p}\right)^{R/c_p}, \tag{13}$$

where p_0 is the reference pressure equal to 1000 hPa, R is the ideal gas constant, and c_p is the specific heat capacity at constant pressure. Similarly, the specific humidity q is used instead of the partial pressure of water vapor e. Equation (3) now reads

$$\mathrm{d}n \;=\; \frac{\mathrm{d}n}{\mathrm{d}\theta}\mathrm{d}\theta + \frac{\mathrm{d}n}{\mathrm{d}q}\mathrm{d}q + \frac{\mathrm{d}n}{\mathrm{d}p}\mathrm{d}p, \tag{14}$$

and (7) is adapted accordingly:

$$n' = A\theta' + Bq' + cp'. \tag{15}$$

New quantities A and B are defined by

$$A = \frac{\mathrm{d}n}{\mathrm{d}\theta} = \frac{\mathrm{d}n}{\mathrm{d}T}\frac{\mathrm{d}T}{\mathrm{d}\theta} = a\left(\frac{p}{p_0}\right)^{R/c_p}, \tag{16}$$

$$B = \frac{\mathrm{d}n}{\mathrm{d}q} = \frac{\mathrm{d}n}{\mathrm{d}e}\frac{\mathrm{d}e}{\mathrm{d}q} = 1.62\; pb. \tag{17}$$

Following the same approach as above, and neglecting pressure fluctuations, C_n^2 is finally found to be related to C_θ^2, C_q^2 and $C_{\theta q}$ by

$$C_n^2 \;=\; A^2\; C_\theta^2 + B^2\; C_q^2 + 2AB\; C_{\theta q}. \tag{18}$$

This result compares to the one obtained for optical wavelengths in [7] using a slightly different approach. Indeed, at optical frequencies, the refractive index is given by [16]

$$n_{\text{opt}} \;=\; 1 + 10^{-6}\;\frac{77.6\;p}{T}\left(1 + \frac{7.52\times 10^{-3}}{\lambda^2}\right), \tag{19}$$

$$\approx 1 + 10^{-6}\;\frac{80\;p}{T}. \tag{20}$$

where the approximation is valid for a wavelength λ equals to $0.5\;\mu$m. Since humidity does not influence the optical refractive index, optical $C_{n,\text{opt}}^2$ is directly related to C_θ^2 by

$$C_{n,\text{opt}}^2 = \tilde{A}^2 C_\theta^2, \tag{21}$$

with $\tilde{A} = \frac{\mathrm{d}n_{opt}}{\mathrm{d}\theta}$ now computed with the definition of the optical refractive index n_{opt}. This gives

$$C^2_{n,\text{opt}} = \left(\frac{80\times10^{-6}p}{T^2}\right)^2\left(\frac{\mathrm{d}T}{\mathrm{d}\theta}\right)^2 C^2_\theta \tag{22}$$

$$= \left(\frac{80\times10^{-6}p}{T\theta}\right)^2 C^2_\theta, \tag{23}$$

that is exactly the result presented in [7], where it is derived from the Tatarskii C^2_n model.

In the following section, (2) and (18) will be used to compute the refractive index structure parameter C^2_n at radio-frequencies, while (20) and (23) will provide the optical refractive index structure parameter $C^2_{n,\text{opt}}$.

III. Presentation of C^2_n models

In this section, two C^2_n models depending on the theoretical developments presented in Section II will be discussed. They are inspired from [19] and [20]. Both models require high-resolution vertical profiles of pressure, (potential) temperature and specific humidity, usually acquired thanks to radiosonde measurements.

A. Direct model - computation of C^2_n

Starting from high-resolution radiosonde data, vertical profiles of pressure, temperature, and specific humidity are re-sampled to a desired vertical resolution, with spacing Δz. From these profiles, the refractive index profile is computed either with (2) or (20). Next, using a vertical window average, the refractive index mean is extracted and the refractive index fluctuations n' are obtained. Assuming to be in the inertial range, computation of $D_n(\rho)$ based on fluctuations n' enables to estimate C^2_n thanks to (8) and (10):

$$C^2_n = \frac{\left\langle \left(n'(\boldsymbol{r}+\boldsymbol{\rho}) - n'(\boldsymbol{r})\right)^2\right\rangle}{\rho^{2/3}}. \tag{24}$$

In practice, the ensemble average in (24) is substituted by a spatial three-points average. It also includes a multiplicative calibration factor c, whose origin is further discussed in the next section.

In the following of this work, this model will be referred to as the *direct model* since the refractive index is computed first, and then C^2_n is extracted. It will be applied to radio-frequency and optical turbulence, depending on the chosen refractive index definition.

B. Indirect model - computations of C^2_θ, C^2_q and $C_{\theta q}$

Instead of relying on the refractive index expressions (2) and (20), expressions of C^2_n (18) and (23) can be used. In this case, knowledge of vertical profiles of potential temperature and specific humidity enables to estimate C^2_θ, C^2_q, and $C_{\theta q}$, as done in (24) for the refractive index. Indeed, fluctuations of θ and q are first computed, then substituted to n' in (24) to obtain the desired structure parameters. As an example, $C_{\theta q}$ is obtained thanks to

$$C_{\theta q} = \frac{\langle(\theta'(\boldsymbol{r}+\boldsymbol{\rho}) - \theta'(\boldsymbol{r}))\,(q'(\boldsymbol{r}+\boldsymbol{\rho}) - q'(\boldsymbol{r}))\rangle}{\rho^{2/3}}. \tag{25}$$

Finally, computed structure parameters are introduced in (18) or (23). This is why this model is referred to as the *indirect model*.

IV. Application to radiosonde measurements

Both models (*direct* and *indirect*) have been applied to high-density radiosonde measurements at Trappes (France) and Hilo (HI, USA) for the year 2020. Data are publicly accessible on the University of Wyoming (UWYO) Atmospheric Science Radiosonde Archive[1]. Radiosondes offer a vertical resolution of approximately 10 meters and are launched twice a day (at 00h00 and 12h00 UTC). For each launch, C^2_n profiles are computed with a vertical spacing $\Delta z = 200$ m. Over the year of 2020, a total of 630 profiles have been computed at Trappes and their average is depicted in Fig. 1. At Hilo, 690 profiles have been computed and averaged to get the results presented in Fig. 2.

Both figures depict the average C^2_n profiles computed with the different models, either at radio-frequencies (RF) or optical frequencies (Opt.). For comparison, the Hufnagel-Valley $5/7$ (HV-$5/7$) model has been added. It is an optical C^2_n model whose definition is [12]

$$C^2_{n,\text{opt}}(z) = 0.00594\left(\frac{w}{27}\right)^2\left(\frac{z}{10^5}\right)^{10}\exp\left(-\frac{z}{1000}\right) + 2.7\times10^{-16}\exp\left(-\frac{z}{1500}\right) + A\exp\left(-\frac{z}{100}\right), \tag{26}$$

with z the altitude, $w = 21$ m/s the root-mean-square high altitude wind speed, and $A = 1.7\times10^{-14}$ m$^{-2/3}$ the ground C^2_n value. The HV-$5/7$ model has been used to calibrate the optical C^2_n model at Trappes in the region between 1 and 4 km of altitude. Indeed, it has been observed that the average computed optical C^2_n profile has exactly the same slope as the HV-$5/7$ profile in this region, and quantitative agreement has been achieved by adding a multiplicative factor $c = 2$ in front of (24). This same factor has been applied to Hilo radiosondes. Its origin may be related to the validity of the inertial range assumption required for (24) to hold, and will be explored in future work.

As a first observation from Figs. 1 and 2, *direct* and *indirect models* provide the same results, showing the consistency of mathematical developments of Section II. Furthermore, the role of humidity fluctuations is clearly identified when comparing RF C^2_n and $C^2_{n,\text{opt}}$. It correlates well with the average relative humidity profiles depicted on the right of both figures. Indeed, humidity is mostly located in the lower

[1] http://weather.uwyo.edu/upperair/bufrraob.shtml

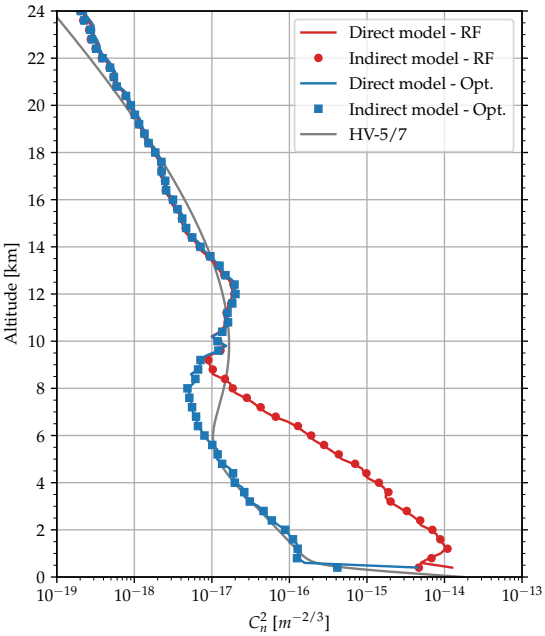

(a) Average C_n^2 profiles

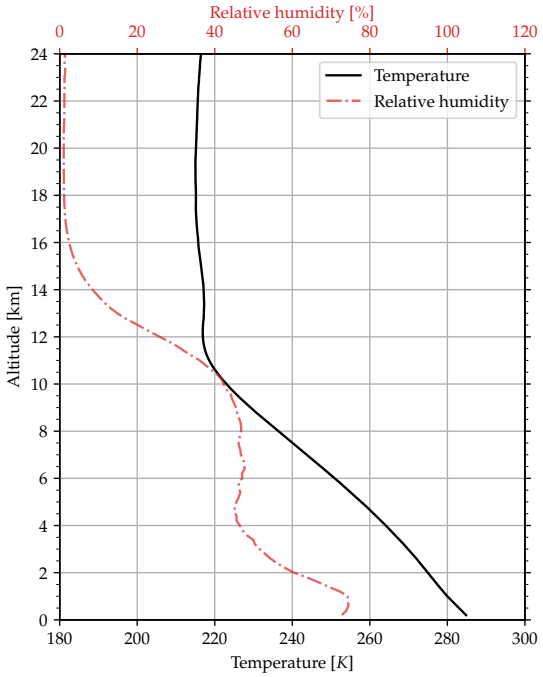

(b) Average temperature and humidity profiles

Fig. 1: Average profiles at Trappes for the year 2020.

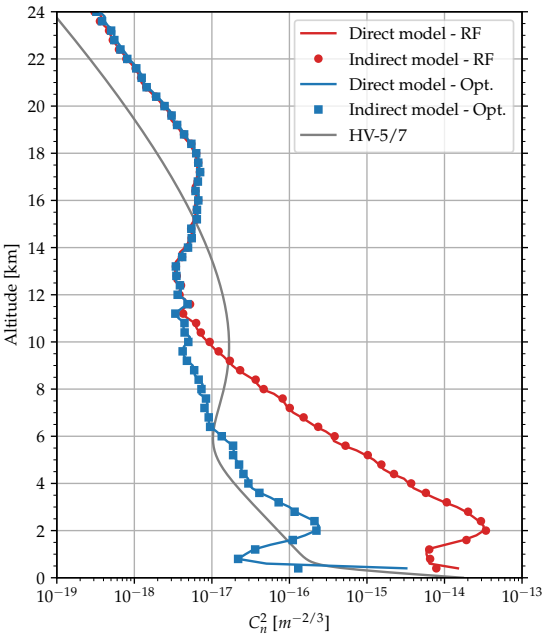

(a) Average C_n^2 profiles

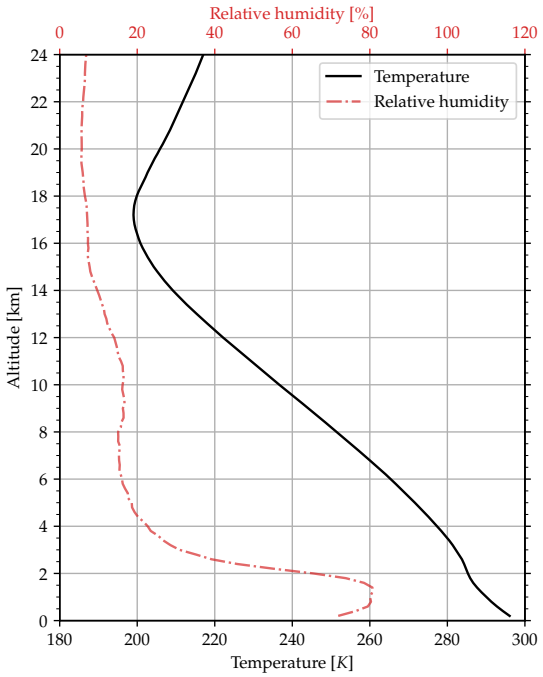

(b) Average temperature and humidity profiles

Fig. 2: Average profiles at Hilo, HI, for the year 2020.

atmospheric layers, impacting C_n^2 in those layers. Starting from slightly below the tropopause (located at $\sim$ 12 km at Trappes and $\sim$ 16 km at Hilo), C_n^2 and $C_{n,\text{opt}}^2$ are equal.

This difference between RF C_n^2 and optical $C_{n,\text{opt}}^2$ profiles has already been identified by [14]. Using a VHF radar, measurements of RF C_n^2 profiles have been acquired, while removing humidity effects leveraged $C_{n,\text{opt}}^2$. In [13], ground measurements of optical and millimeter wave C_n^2 showed a difference of two orders of magnitude between both values. This is consistent with the differences between modelled C_n^2 and $C_{n,\text{opt}}^2$ near the ground for both locations.

Other differences between average C_n^2 profiles at Trappes and Hilo include the altitude of the tropopause and the presence of isolated turbulent layers. Tropopause altitude at Trappes is close to 12 kilometers as seen from the bump in the C_n^2 profile. At Hilo, the tropopause is above 16 km of altitude. In both cases, there is a mismatch with the HV-$5/7$ profile explained by the difference in locations, since the Hufnagel-Valley model is based on measurements performed in New Mexico, USA, and not at Trappes or Hilo. Regarding Hilo, there are often strong temperature inversion layers arising around 2 kilometers of altitude. This induces a peak in the C_θ^2 profile, and thus in the (average) C_n^2 profiles at radio and optical frequencies.

V. Conclusion

Two approaches enabling to estimate C_n^2 profiles at radio and optical frequencies have been presented. They rely on the statistical definition of the refractive index structure parameter, and enable to obtain time- and location-dependent profiles determined by meteorological quantities (i.e. pressure, temperature, and humidity).

The approaches have been compared and applied to high-density radiosonde observations at Trappes (France) and Hilo (HI, USA). Based on the obtained results, differences between C_n^2 profiles at radio and optical frequencies have been found to be related to humidity fluctuations in the lower atmospheric layers.

At the date of publication, the C_n^2 model at optical frequencies has been validated with measurements. This will be the topic for a future publication. However, as part of future work, validation of the radio-frequency C_n^2 model will also be conducted. It remains challenging since no scintillation or C_n^2 profile measurements are available at sites where high-resolution radiosonde observations have been collected [1]. Furthermore, sensitivity studies to the accuracy of temperature and humidity measurements will also be conducted.

References

[1] D. Vanhoenacker-Janvier, C. Oestges, and A. Martellucci, "Prediction of scintillation cumulative statistics using classical and high resolution radiosoundings," in *2006 First European Conference on Antennas and Propagation*, pp. 1–5, IEEE, 2006.

[2] F. S. Marzano, C. Riva, A. Banich, and F. Clivio, "Assessment of model-based scintillation variance prediction on long-term basis using italsat satellite measurements," *International journal of satellite communications*, vol. 17, no. 1, pp. 17–36, 1999.

[3] Y. Karasawa, M. Yamada, and J. E. Allnutt, "A new prediction method for tropospheric scintillation on earth-space paths," *IEEE transactions on antennas and propagation*, vol. 36, no. 11, pp. 1608–1614, 1988.

[4] M. M. van de Kamp, J. K. Tervonen, E. T. Salonen, and J. P. Baptista, "Improved models for long-term prediction of tropospheric scintillation on slant paths," *IEEE Transactions on antennas and propagation*, vol. 47, no. 2, pp. 249–260, 1999.

[5] A. Ishimaru, *Wave propagation and scattering in random media*, vol. 2. Academic press New York, 1978.

[6] V. I. Tatarskii, "The effects of the turbulent atmosphere on wave propagation," *Jerusalem: Israel Program for Scientific Translations, 1971*, 1971.

[7] T. Cherubini and S. Businger, "Another look at the refractive index structure function," *Journal of applied meteorology and climatology*, vol. 52, no. 2, pp. 498–506, 2013.

[8] A. M. Marziani, C. Riva, F. Consalvi, E. R. Restuccia, and F. S. Marzano, "Clear-air scintillation analysis of q-band alphasat link at spino d'adda using radiosounding data," in *2017 11th European Conference on Antennas and Propagation (EUCAP)*, pp. 15–19, IEEE, 2017.

[9] H. Vasseur, "Prediction of tropospheric scintillation on satellite links from radiosonde data," *IEEE Transactions on Antennas and Propagation*, vol. 47, no. 2, pp. 293–301, 1999.

[10] C. Pereira, C. Ghiringhelli, and D. Vanhoenacker-Janvier, "Sensitivity of tropospheric scintillation models to the accuracy of radiosonde data," in *2015 9th European Conference on Antennas and Propagation (EuCAP)*, pp. 1–4, IEEE, 2015.

[11] F. Roddier, "V the effects of atmospheric turbulence in optical astronomy," in *Progress in optics*, vol. 19, pp. 281–376, Elsevier, 1981.

[12] L. C. Andrews and R. L. Phillips, *Laser Beam Propagation through Random Media, Second Edition*. SPIE Press, 2005.

[13] R. J. Hill, R. A. Bohlander, S. F. Clifford, R. W. McMillan, J. Priestly, and W. Schoenfeld, "Turbulence-induced millimeter-wave scintillation compared with micrometeorological measurements," *IEEE Transactions on Geoscience and Remote Sensing*, vol. 26, no. 3, pp. 330–342, 1988.

[14] F. Eaton, W. Peterson, J. Hines, K. Peterman, R. Good, R. Beland, and J. Brown, "Comparisons of vhf radar, optical, and temperature fluctuation measurements ofc n 2, r 0 andθ 0," *Theoretical and applied climatology*, vol. 39, no. 1, pp. 17–29, 1988.

[15] B. R. Bean and E. Dutton, *Radio meteorology*, vol. 92. Superintendentof Documents, US GovernmentPrint. Office, 1966.

[16] A. D. Wheelon, *Electromagnetic scintillation: volume 1, geometrical optics*. Cambridge University Press, 2001.

[17] E. E. Gossard, "Refractive index variance and its height distribution in different air masses," *Radio Science*, vol. 12, no. 1, pp. 89–105, 1977.

[18] A. Moene, "Effects of water vapour on the structure parameter of the refractive index for near-infrared radiation," *Boundary-layer meteorology*, vol. 107, no. 3, pp. 635–653, 2003.

[19] C. Pereira, D. Vanhoenacker-Janvier, N. Jeannin, L. Castanet, and A. Martellucci, "Simulation of tropospheric scintillation on leo satellite link based on space-time channel modeling," in *The 8th European Conference on Antennas and Propagation (EuCAP 2014)*, pp. 3516–3519, IEEE, 2014.

[20] C. Wilson and E. Fedorovich, "Direct evaluation of refractive-index structure functions from large-eddy simulation output for atmospheric convective boundary layers," *Acta Geophysica*, vol. 60, no. 5, pp. 1474–1492, 2012.